ISSN 2176-5480

22nd International Congress of Mechanical Engineering (COBEM 2013)
November 3-7, 2013, Ribeirão Preto, SP, Brazil

EXPERIMENTAL EVALUATION OF COMPACT MICROCHANNEL HEAT EXCHANGERS WITH LOUVER FINS

Paulo C. Sedrez
Jader R. Barbosa Jr.
POLO - Research Laboratories for Emerging Technologies in Cooling and Thermophysics, Department of Mechanical Engineering, Federal University of Santa Catarina, Florianópolis, SC, 88040-900, Brazil
E-mail: jrb@polo.ufsc.br

Guilherme B. Ribeiro
Embraco Compressors, Joinville, SC, Brazil
E-mail: Guilherme_B_Ribeiro@embraco.com.br

Abstract. *The thermal-hydraulic performance of two aluminum microchannel heat exchangers with louver fins on the air-side was evaluated experimentally. An open-loop wind-tunnel calorimeter was used to obtain experimental data on the air-side pressure drop and thermal conductance. The data were correlated in terms of the Darcy friction factor, the Colburn j-factor and the Reynolds number based on the spacing between the louvers, for air mass flow rates ranging from 33 to 67 m^3/h. The average absolute deviations associated with the proposed correlations were 1% for the Colburn j-factor and 6% for the friction factor.*

Keywords: *Enhanced heat transfer, compact heat exchanger, louver fins, correlation, heat transfer, friction factor.*

1. INTRODUCTION

A gas-liquid heat exchanger is said to be compact when the surface area density (i.e., the area per unit volume) exceeds 700 m^2/m^3 (Kakaç and Liu, 2002). Compact heat exchangers are commonly used in applications involving gases, since the large external surface area per unit volume compensates the low heat transfer coefficients associated with the air flow. A large area density on the air side is usually obtained by means of extended surfaces (fins). Louver fins are a type of interrupted fins which are known for its ability to increase the heat transfer coefficient two to four times that for the corresponding plain (uncut) fin surface (Shah and Sekulić, 2003). Surface interruptions break the growth of the boundary layer on the enhanced (extended) surface. As a result, the thinner boundary layers give rise to higher heat transfer coefficients. However, this heat transfer increase is followed by an increase in the friction factor due to flow separation and recirculation effects.

The friction and heat transfer characteristics of flows through louver fins have been widely discussed in the literature. Webb and Kim (2005) reviewed the experimental and modeling efforts aimed at the description of the effect geometry parameters such as the louver pitch and louver angle on the combined effect of heat transfer and pressure drop. Heat transfer and pressure drop correlations have been proposed by several authors (Davenport, 1983; Chang and Wang, 1997; Chang *et al.*, 2000; Park and Jacobi, 2009), which cover a wide range of geometry parameters and operating conditions.

The objective of this paper is to evaluate experimentally the air-side thermal-hydraulic performance of two compact flat-tube microchannel heat exchangers in which louver fins were employed to enhance the external heat transfer coefficient. The experimental data were obtained in an open-loop wind tunnel calorimeter available at the Federal University of Santa Catarina. A distinctive feature of the heat exchangers evaluated in the present work is the presence of a single louver bank. While the majority of the data available in the literature is for the double louver bank configuration (Park and Jacobi, 2009), there is a dearth of experimental data for single louver bank fins. The only reported data in the literature are those by Achaichia and Cowell (1988). Therefore, the existing correlations fail to predict the single louver bank heat exchanger surface with reasonable accuracy. Despite the limited number of data points generated in the present study, a simple correlation was proposed, which correlated the data with absolute average deviations of 1% for the Colburn j-factor and 6% for the Darcy friction factor. The correlations used the louver spacing as the characteristic length in the Reynolds number.

The paper is structured as follows. Section 2 describes the heat exchangers, the experimental facility and the experimental procedure. The data regression is presented in Section 3. Section 4 presents the results and, Section 5, the final conclusions.

ISSN 2176-5480

2. EXPERIMENTAL WORK

2.1 Heat exchanger prototypes

The heat exchanger samples investigated in this work are presented in Fig. 1. They consist of a cross-flow aluminum coil (flat-tube), which has four circular microchannels with an internal diameter of 0.8 mm. The aluminum louver fins are brazed to the external surface of the coil, as shown in detail in Fig. 1(b). The single difference between the samples shown in Fig. 1(a) is the number of tube (coil) passes in the direction normal to the air flow. Sample T01 (right) has 6 passes, and samples T02 (center) and T03 (left) have 8 and 10 passes, respectively. The fin density, the fin thickness and the heat exchanger length (in the direction of the air flow) are the same for all samples. The surface area per unit volume is approximately 800 m^2/m^3 for all samples. In the present paper, only the results associated with samples T01 and T02 are presented. The heat exchangers were supplied by Embraco.

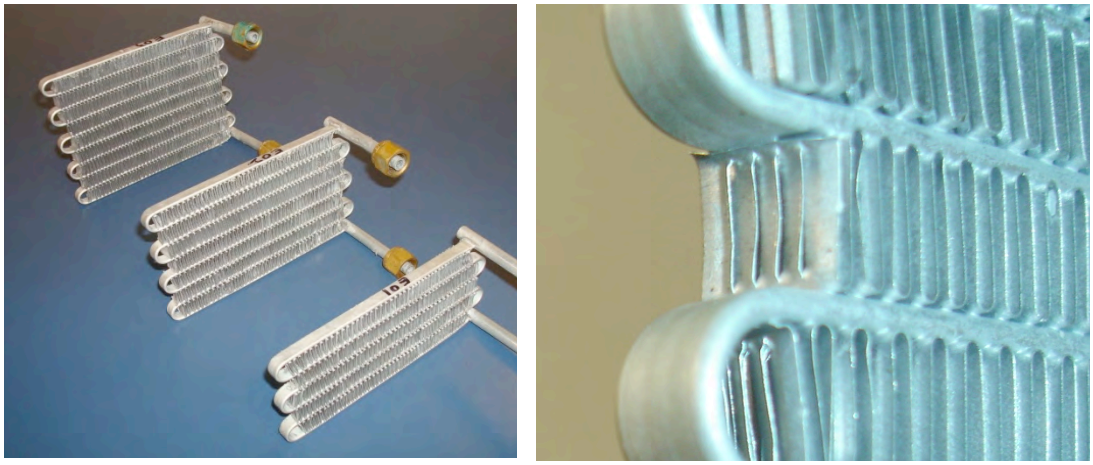

(a) General view of the samples. (b) Louver fin (in detail).

Figure 1. Heat exchangers samples.

The geometric parameters of the louver fin (see also Table 1), which were measured in the present study with a caliper rule, are presented in Figs. 2 and 3. The values of the fin thickness, louver angle and internal diameter of the microchannels were supplied by Embraco. It is important to mention that the fin investigated here is of the single-louver bank type, as illustrated in Fig. 3(a).

Table 1. Summary of the characteristics of the heat exchanger prototypes.

Geometric parameter	Value
T_D	7.5
H	8.0
F_D	8.0
L_L	6.0
T_P	10.0
F_P	1.35
α	23°

2.2 Experimental facility

The open-loop wind tunnel facility used in the heat transfer tests (Fig. 4) has been described in detail in previous works (Barbosa *et al.*, 2009; Waltrich *et al.*, 2011; Pussoli *et al.*, 2012) and, for completeness, only its main features will be reported here. The facility was constructed from a double layer of steel plates, and a 100-mm thick layer of glass wool was inserted between the plates for thermal insulation. The air-side instrumentation is comprised by a 51-W speed controlled fan, a set of 5 aluminum nozzles with diameters ranging from 19.05 mm to 31.75 mm, 2 differential pressure transducers to measure the air-side pressure drop in the evaporator and in the nozzles and nine T-type thermocouples for the air temperature measurements upstream and downstream of the test section. The temperature fluctuation of the ambient air entering the calorimeter was controlled to $\pm 0.1°C$ before entering the wind tunnel (Waltrich *et al.*, 2011).

ISSN 2176-5480

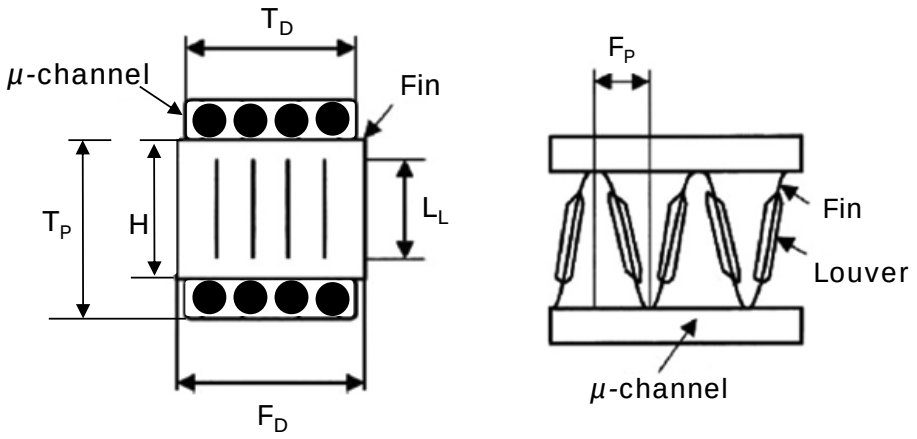

(a) Side view (the air flow is normal to the microchannels). (b) Frontal view of the louver fins.

Figure 2. Schematic diagram of the louver fins and microchannels.

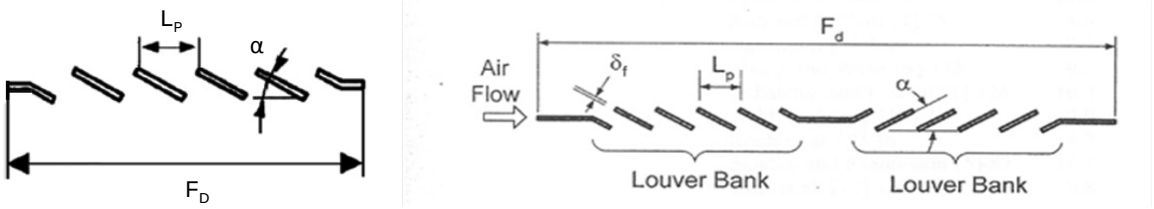

(a) Single-louver bank fin. (b) Double-louver bank fin.

Figure 3. Cross-section view of the louver fins (Adapted from Park and Jacobi, 2009).

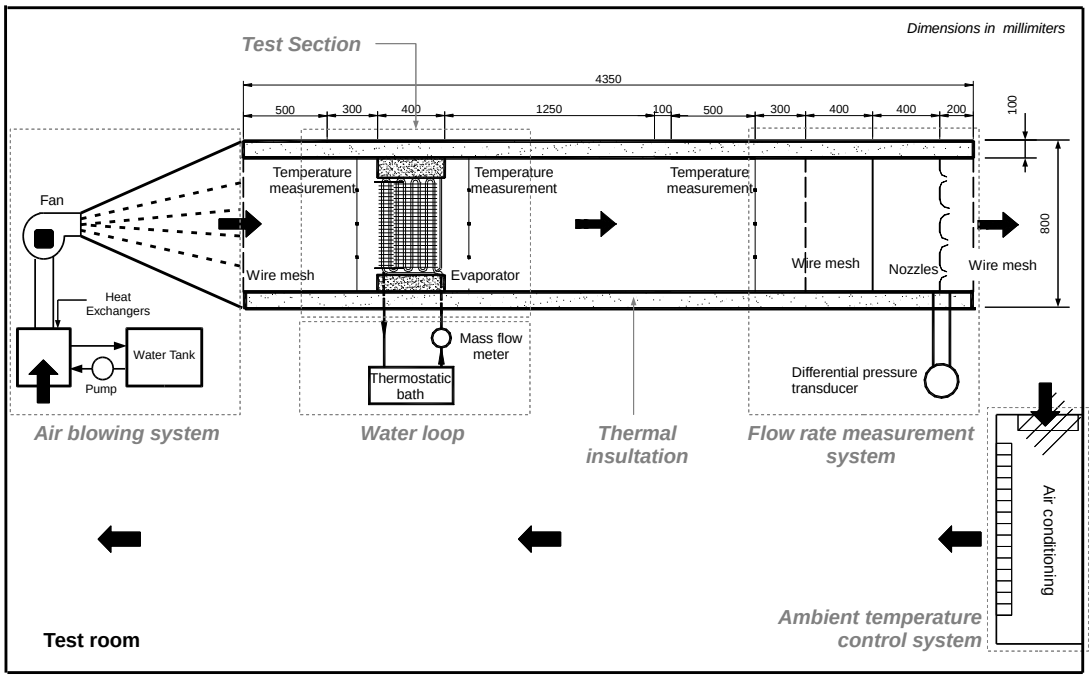

Figure 4. Schematic diagram of the experimental facility (Waltrich *et al.*, 2011).

The air flow rate is calculated via the measured pressure drop in the calibrated nozzles according to the procedure recommended by ANSI/ASHRAE (1999). Wire meshes are employed to make the flow uniform in the inlet and exit sections and also upstream of the air flow nozzles.

The measurement of the air temperature upstream and downstream of the heat exchanger is carried out by three thermocouples placed upstream and six placed downstream of it. The thermocouples are embedded into small copper blocks

ISSN 2176-5480

(diameter and height of 10 mm) to minimize temperature oscillations during the measurements. The air-side static pressure drop is measured by mounting perforated hoses (spacing between adjacent holes of 25 mm) on two grooves machined on the bottom wall of the test section (one groove is located upstream and the other downstream of the evaporator). The grooves are perpendicular to the main flow direction and their depth is such that the pressure taps are at the same level as the bottom wall. The adjoining surfaces are leveled with silicone glue to avoid disturbing the flow in the vicinity of the pressure taps. One end of each hose is connected to the differential pressure transducer while the other end is sealed. The accuracy of each pressure transducer is $\pm$ 0.5 % of the full scale ($\sim$500 Pa for the heat exchanger transducer and $\sim$995 Pa for the nozzle transducer).

The main function of the water loop is to circulate water at controlled temperatures and flow rates through the evaporator. The following components make up the water circuit: a 4 L/min (max.) speed-controlled rotary pump; a 100°C (max.), $\pm$ 0.1°C accuracy, thermostatic bath; and a 5 L/min (max.), 1.4% full scale accuracy, turbine flow meter. The loop is thermally insulated and T-type immersion thermocouples ($\pm$ 0.2°C) are placed immediately upstream and downstream of the heat exchanger.

2.3 Experimental procedure

The apparatus is switched on, the inlet water temperature is set and approximately 10 minutes are required for it to stabilize. The desired air flow rate is adjusted and the water flow rate is set in order to provide a temperature range (difference between the inlet and outlet temperatures) of the order of 5°C. Approximately 50 to 80 minutes — depending on the air flow rate — are required in order to reach steady-state. The steady-state criterion has been established as follows: each parameter is averaged over a 30-minute interval (total of 452 data points) and the standard deviation associated with its signal is calculated. If the absolute value of the difference between the reading at the beginning of the sampling interval (t = 0) and at the end (t = 30 min) is less than 3 times the standard deviation, the test is considered stabilized.

3. DATA REGRESSION

3.1 Heat transfer

The overall thermal conductance is given by:

$$UA = \frac{\dot{Q}}{F\Delta T_{lm,cc}} \tag{1}$$

where $\dot{Q}$ is the heat transfer rate calculated as the arithmetic average between the heat transfer rates measured on the air and water sides. Thus:

$$\dot{Q} = \frac{1}{2}\left(\dot{Q}_a + \dot{Q}_w\right) \tag{2}$$

where:

$$\dot{Q}_a = \rho_a \dot{V}_a c_{p,a}\left(T_{a,out} - T_{a,in}\right) \tag{3}$$

$$\dot{Q}_w = \dot{m}_w c_{p,w}\left(T_{w,in} - T_{w,out}\right) \tag{4}$$

The counter-current log-mean temperature difference, $\Delta T_{lm,cc}$, and the cross-flow correction factor, F, are given by:

$$\Delta T_{lm,cc} = \frac{\left(T_{w,in} - T_{a,in}\right) - \left(T_{w,out} - T_{a,out}\right)}{\ln\left(\frac{T_{w,in} - T_{a,in}}{T_{w,out} - T_{a,out}}\right)} \tag{5}$$

and:

$$F = \frac{\ln\left[\frac{(1-RP)}{(1-P)}\right]}{NTU\,(1-R)} \tag{6}$$

ISSN 2176-5480

where:

$$R = \frac{T_{w,in} - T_{w,out}}{T_{a,out} - T_{a,in}} \tag{7}$$

$$P = \frac{T_{a,out} - T_{a,in}}{T_{w,in} - T_{a,in}} \tag{8}$$

$$NTU = \frac{T_{a,out} - T_{a,in}}{\Delta T_{lm,cc}} \tag{9}$$

and the subscripts a and w stand for the air and water streams, respectively.

The air-side heat transfer coefficient is calculated subtracting the internal convection and the solid wall heat transfer resistances from the overall thermal resistance as follows:

$$\eta_o \overline{h}_o = \left[\left(\frac{1}{UA} - \frac{1}{\overline{h}_i A_i} - \frac{e_s}{k_s A_s} \right) A_o \right]^{-1} \tag{10}$$

where η_o is the external overall surface efficiency, k_s is the thermal conductivity of the solid wall material (aluminum), e_s is the thickness of the coil solid wall, and A_i, A_s and A_o are, respectively, the surface area of the microchannels, the surface area of the solid wall (aluminum coil) and the surface area of the solid material (coil plus fins) in direct contact with the air (Shah and Sekulić, 2003). The thermal resistance of the solid wall is generally much smaller than the other two resistances and can be neglected. The internal heat transfer coefficient was calculated based on the Gnielinski correlation as follows (Lienhard and Lienhard, 2001):

$$Nu_{d_i} = \frac{\overline{h}_i d_i}{k_w} = \frac{f_w/8 \left(Re_{d_i} - 10^3 \right) Pr_w}{1 + 12.7 \left(f_w/8 \right)^{1/2} \left(Pr_w^{2/3} - 1 \right)} \tag{11}$$

where Pr_w and Re_{d_i} are the water-side Prandtl and Reynolds numbers, respectively. The latter is defined by:

$$Re_{d_i} = \frac{G_w d_i}{\mu_w} \tag{12}$$

where μ_w is the water dynamic viscosity, d_i is the microchannel diameter and G_w is the water mass flux (i.e., the mass flow rate per unit cross-section area) *per channel*. The water-side friction factor was calculated via the Petukov correlation given by (Lienhard and Lienhard, 2001):

$$f_w = \left[0.79 \ln \left(Re_{d_i} \right) - 1.64 \right]^{-2} \tag{13}$$

The external overall surface efficiency was incorporated into the definition of the Colburn j-factor. Thus:

$$j = \frac{L_P}{k_a} \frac{\eta_o \overline{h}_o}{Re_a Pr_a^{1/3}} \tag{14}$$

As can be seen from Eq. (14), the louver pitch was defined as the characteristic length scale (Park and Jacobi, 2009). Thus, the air-side Reynolds number is given by:

$$Re_a = \frac{G_a L_P}{\mu_a} \tag{15}$$

where G_a is the air-side mass flux defined as:

$$G_a = \rho_a V_{max} \tag{16}$$

ISSN 2176-5480

where V_{max} is the maximum air velocity that takes place in the minimum free-flow area cross-section, A_{min}. A_{min} is calculated based on the geometry parameters of the heat exchangers as follows (Shah and Sekulić, 2003):

$$A_{min} = A_f - N_{fin}\delta_{fin}H_{fin} - N_{tube}\delta_{tube}H_{tube} \tag{17}$$

where A_f is the heat exchanger face area and the second and third terms are the portions of the face area occupied by the fins and tubes, respectively.

3.2 Pressure drop

The Darcy friction factor for the air flow is calculated from the following relationship:

$$f = \frac{A_{min}}{A_o}\frac{\rho_a}{\rho_{a,in}}\left[\frac{2\Delta p_a \rho_{a,in}}{G_a^2} - \left(1+\sigma^2\right)\left(\frac{\rho_{a,in}}{\rho_{a,out}} - 1\right)\right] \tag{18}$$

where $\rho_{a,in}$ and $\rho_{a,out}$ are the air density corresponding to the inlet and outlet sections. ρ_a is the arithmetic average of the inlet and outlet air densities. σ is the ratio of the minimum free-flow area, A_{min}, and the face area, A_f. Δp_a is the measured air-side pressure drop.

4. RESULTS

4.1 Experimental results

As mentioned above, only the samples T01 and T02 have been tested experimentally. For each heat exchanger, five air flow rates, ranging between 34 to 67 m^3/h, have been evaluated. The experimental data are summarized in Table 2. Figures 5 and 6 present the behavior of the air-side pressure drop and of the overall thermal conductance as a function of the air flow rate for both heat exchanger samples.

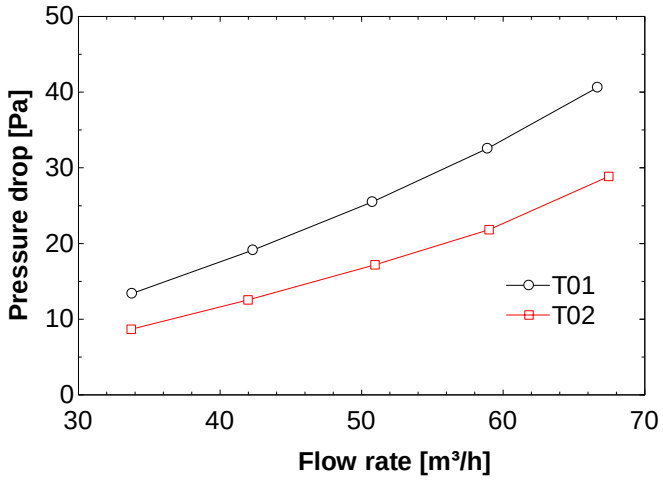

Figure 5. Behavior of the air-side pressure drop as a function of the air flow rate for the two heat exchangers.

As expected, the pressure drop increases with the air flow rate (Fig. 5). For a given air flow rate, the pressure drop is larger for the sample T01 because of its smaller frontal area, which gives rise to larger air velocities in the heat exchanger. The overall thermal conductance of the sample T02, on the other hand, is larger because of its larger heat transfer surface area, as seen in Fig. 6.

4.2 Data regression

The values of j and f derived from the experimental data are presented in Table 3, as a function of the air-side Reynolds number based on the louver pitch. The same data are presented in graphical form in Fig. 7.

As can be seen from Fig. 7, the j and f data for the two heat exchanger samples seem to collapse into single trend lines, indicating that the only independent parameter is, in fact, Re_a. This behavior was somewhat expected, since the tube dimensions and the fin geometry were identical for both heat exchangers. The only difference between the samples is the number of tube passes normal to the air flow direction. This obviously results in different face, minimum free-flow and

ISSN 2176-5480

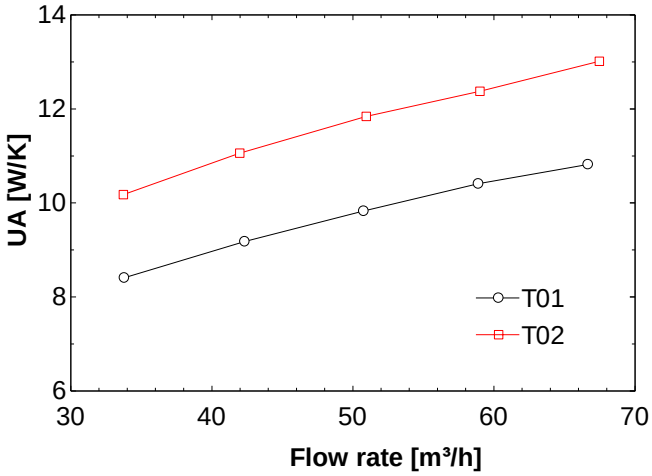

Figure 6. Behavior of the overall thermal conductance as a function of the air flow rate for the two heat exchangers.

Table 2. Experimental data.

	Air-side				Water-side			Results	
	Flow rate (ft^3/min)	Flow rate (m^3/h)	Inlet temperature (°C)	Outlet temperature (°C)	Mass flow rate (kg/h)	Inlet temperature (°C)	Outlet temperature (°C)	Δp_a (Pa)	Q (W)
T01	19.9	33.8	19.0	26.8	22.4	37.3	33.3	13.4	97.2
	24.9	42.3	19.0	25.9	22.3	37.0	32.7	19.1	105.9
	29.9	50.8	19.0	25.3	22.2	37.0	32.3	25.5	114.4
	34.7	58.9	19.2	24.9	21.9	36.7	31.8	32.6	118.2
	39.2	66.7	19.2	24.2	21.3	36.5	31.3	40.6	121.4
T02	19.9	33.7	18.9	27.1	20.9	36.4	31.8	8.7	103.0
	24.7	42.0	19.0	26.4	21.0	36.2	31.2	12.6	112.4
	30.0	50.9	19.0	25.7	21.2	36.0	30.7	17.2	120.7
	34.7	59.0	19.0	24.9	20.5	35.6	30.0	21.8	123.7
	39.7	67.5	19.1	24.3	20.8	35.5	29.7	28.9	129.4

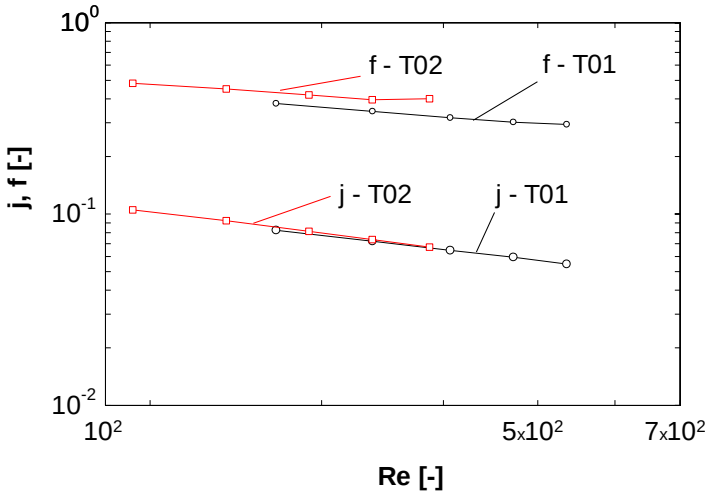

Figure 7. Experimental data regression in terms of the friction and Colburn j-factors as a function of the air-side Reynolds number.

external surface areas, but their effects are eliminated when the experimental data are correlated in terms of the proposed dimensionless parameters.

The larger scatter in the friction factor data in comparison with those for the Colburn j-factor is possibly due to the experimental uncertainty associated with the pressure drop measurement. The pressure transducer used in the experimental apparatus had a full scale of 500 Pa. The calculated experimental uncertainty of the air pressure drop was $\pm$ 2.8 Pa, which

ISSN 2176-5480

Table 3. Summary of the data regression.

	Re_a	j	f
T01	269.6	0.0822	0.3783
	338.6	0.0720	0.3437
	406.8	0.0646	0.3184
	472.3	0.0595	0.3020
	535.7	0.0547	0.2940
T02	192.0	0.1052	0.4827
	239.4	0.0923	0.4512
	291.2	0.0813	0.4191
	338.2	0.0736	0.3960
	387.2	0.0673	0.4008

is relatively large compared to the magnitude of the measured pressure drop in the heat exchangers under the present test conditions (see Table 1).

The experimental data were correlated using simple power-law relationships as follows:

$$j = ARe_a^B \tag{19}$$

and:

$$f = CRe_a^D \tag{20}$$

where the constants A, B, C and D were determined via a least-squares minimization method. Graphical representations of the data correlation are shown in Fig. 8 and the values of the constants are presented in Table 4. Table 5 shows the error associated with the empirical correlations for each data point. The average errors for j and f were 0.95% and 5.73%, respectively.

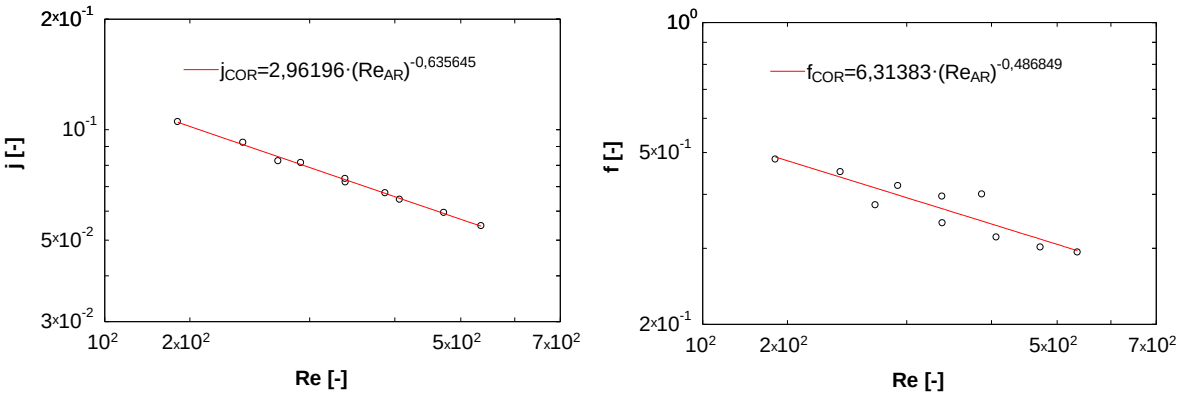

(a) Colburn j-factor.

(b) Darcy friction factor.

Figure 8. Prediction of the experimental data by the empirical correlations.

Table 4. Values of the empirical constants in Eqs. (19) and (20).

Constant	Value
A	2.9620
B	-0.6356
C	6.3138
D	-0.4868

ISSN 2176-5480

Table 5. Summary of errors of the empirical correlations.

	Re_a	j_{exp}	f_{exp}	j_{cor}	f_{cor}	Err j (%)	Err f (%)
T01	269.6	0.0822	0.3783	0.0844	0.4139	−2.7	−9.4
	338.6	0.0720	0.3437	0.0730	0.3704	−1.4	−7.8
	406.8	0.0646	0.3184	0.0650	0.3388	−0.7	−6.4
	472.3	0.0595	0.3020	0.0591	0.3150	0.6	−4.3
	535.7	0.0547	0.2940	0.0546	0.2963	0.3	−0.8
T02	192.0	0.1052	0.4827	0.1048	0.4883	0.4	−1.2
	239.4	0.0923	0.4512	0.0911	0.4385	1.3	2.8
	291.2	0.0813	0.4191	0.0804	0.3987	1.1	4.9
	338.2	0.0736	0.3960	0.0731	0.3707	0.7	6.4
	387.2	0.0673	0.4008	0.0671	0.3470	0.3	13.4

5. CONCLUSIONS

The air-side heat transfer and pressure drop characteristics of microchannel heat exchangers with louver fins have been evaluated in this paper. The experimental data were generated in a wind tunnel calorimeter for air mass flow rates ranging from 33 to 67 m^3/h. The most distinctive feature of the heat exchangers evaluated here is that the louver fins contain a single louver bank. Empirical correlations for the Colburn j-factor and for the Darcy friction factor as a function of the fin pitch Reynolds number were developed. The average absolute deviations associated with the proposed correlations were 1% for the Colburn j-factor and 6% for the friction factor.

6. ACKNOWLEDGEMENTS

The authors would like to thank Embraco and the CNPq through grant No. 573581/2008-8 (National Institute of Science and Technology in Cooling and Thermophysics) for the financial support.

7. REFERENCES

Achaichia, A. and Cowell, T.A., 1988. "Heat transfer and pressure drop characteristics of flat tube and louvered plate fin surfaces". *Experimental Thermal and Fluid Science*, Vol. 1, pp. 147–157.

ANSI/ASHRAE, 1999. "Standard 51 - laboratory methods of testing fans for rating". American Society of Heating, Refrigeration and Air Conditioning Engineers, Atlanta, GA, USA.

Barbosa Jr., J.R., Melo, C., Hermes, C.J.L. and Waltrich, P.J., 2009. "A study of the air-side heat transfer and pressure drop characteristics of tube-fin 'no-frost' evaporators". *Applied Energy*, Vol. 86, pp. 1484–1491.

Chang, Y.J., Hsu, K.C., Lee, Y.T. and Wang, C.C., 2000. "A generalized friction correlation for louver fin geometry". *International Journal of Heat and Mass Transfer*, Vol. 43, pp. 2237–2243.

Chang, Y.J. and Wang, C.C., 1997. "A generalized heat transfer correlation for louver fin geometry". *International Journal of Heat and Mass Transfer*, Vol. 40, pp. 533–544.

Davenport, C.J., 1983. "Correlations for heat transfer and flow friction characteristics of louver fin". In *Heat Transfer – Seattle 1983*. Vol. AIChE Symposium Series, No. 225, pp. 19–27.

Kakaç, S. and Liu, H., 2002. *Heat Exchangers: Selection, Rating and Thermal Design*. CRC Press, 2nd edition.

Lienhard, J.H. and Lienhard, J.H., 2001. *A Heat Transfer Textbook*. Phlogiston Press, 3rd edition.

Park, Y.G. and Jacobi, A.M., 2009. "Air-side heat transfer and friction correlations for flat-tube louver-fin heat exchangers". *Journal of Heat Transfer, Transactions of the ASME*, Vol. 131, pp. 021801–1–021801–12.

Pussoli, B.F., Barbosa Jr., J.R., da Silva, L.W. and Kaviany, M., 2012. "Heat transfer and pressure drop characteristics of peripheral-finned tube heat exchangers". *International Journal of Heat and Mass Transfer*, Vol. 55, pp. 2835–2843.

Shah, R.K. and Sekulić, D.P., 2003. *Fundamentals of Heat Exchanger Design*. John Wiley & Sons.

Waltrich, P.J., Barbosa Jr., J.R., Melo, C. and Hermes, C.J.L., 2011. "Air-side heat transfer and pressure drop characteristics of accelerated flow evaporators". *International Journal of Refrigeration*, Vol. 34, pp. 484–497.

Webb, R.L. and Kim, N.H., 2005. *Principles of Enhanced Heat Transfer*. Taylor & Francis, 2nd edition.

8. RESPONSIBILITY NOTICE

The authors are the only responsible for the printed material included in this paper.